Preliminary Performance Assessment of a Fuel-Cell Powered Hypersonic Airbreathing Magjet[1]

Bernard Parent and In-Seuck Jeung
Dept. of Aerospace Engineering, Seoul National University
Seoul 151-744, Korea
bernard@snu.ac.kr, enjis@snu.ac.kr

Keywords: Airbreathing jet propulsion, Magnetoplasmadynamics, Hypersonic flight

Abstract

A variant of the magnetoplasma jet engine (magjet) is here proposed for airbreathing flight in the hypersonic regime. As shown in Figure 1, the engine consists of two distinct ducts: the high-speed duct, in which power is added electromagnetically to the incoming air by a momentum addition device, and the fuel cell duct in which the flow stagnation temperature is reduced by extracting energy through the use of a magnetoplasmadynamic (MPD) generator. The power generated is then used to accelerate the flow exiting the fuel cells with a fraction bypassed to the high-speed duct. The analysis is performed using a quasi one-dimensional model neglecting the Hall and ion slip effects, and fixing the fuel cell efficiency to 0.6. Results obtained show that the specific impulse of the magjet is at least equal to and up to 3 times the one of a turbojet, ramjet, or scramjet in their respective flight Mach number range. Should the air stagnation temperature in the fuel cell compartment not exceed 5 times the incoming air static temperature, the maximal flight Mach number possible would vary between 6.5 and 15 for a magnitude of the ratio between the Joule heating and the work interaction in the MPD generator varied between 0.25 and 0.01, respectively. Increasing the mass flow rate ratio between the high speed and fuel cell ducts from 0.2 to 20 increases the engine efficiency by as much as 3 times in the lower supersonic range, while resulting in a less than 10% increase for a flight Mach number exceeding 8.

Introduction

Chemical airbreathing jet engines powering present-day aircraft provide thrust through conversion of the heat added chemically into work, which is accomplished by compressing and expanding the fluid before and after the heat addition, respectively. While this has proven to be a viable concept for flight over a limited Mach number range, extending the flight Mach number envelope of chemical airbreathing engines is not a trivial task. Difficulties originate from the complicated compression process in the inlet which needs to be accomplished with minimal losses. To minimize losses while maintaining a high pressure in the combustor, radical variations in the design/geometry of the engine are needed as the aircraft accelerates from rest to hypersonic speeds.

This prompted the development of substantially different engine designs such as the turbojet, the ramjet, and the scramjet to cover the flight Mach number envelopes 0–3, 3–7, and 7–15, respectively. It follows that for a chemical airbreathing engine to operate from rest to high speeds, the different designs must be combined into one or somehow substituted to one another during flight. Adding to the challenge is the extreme heat load characteristic of hypersonic flight effectively rendering any type of mechanical control on the engine geometry a particularly challenging endeavour.

To circumvent the difficulties associated with geometry variations of chemical airbreathing jet engines over a wide flight Mach number range, a novel propulsion concept dubbed the *magnetoplasma jet* engine, or *magjet*, is proposed in Ref. 1. Contrarily to chemical jet engines which are characterized by energy addition to the flow as *heat*, the magjet is advantaged by electromagnetic energy addition to the flow directly as *work*, with the power source being a stack of fuel cells. By not requiring the flow to be compressed and expanded, the magjet can operate with little variations in geometry. Another advantage includes a higher specific impulse which is reported[1] to be 20% greater to 3 times the one of a turbojet, ramjet, and scramjet over their respective Mach number range of operation. Further, the flow temperature and pressure are observed not to vary significantly from the freestream conditions throughout the engine, hence possibly reducing the heat loads as well as the noise level.

However, the magjet performance is assessed in Ref. 1 assuming that the fuel cells can obtain somehow the necessary oxygen to operate from the ambiant air. Below a flight Mach number of about 2, this is expected to be feasible due to the minimal heat loads on the fuel cells. On the other hand, the latter would need substantial cooling to operate for hypersonic flight. As it might be technically difficult to achieve such cooling while maintaining a high fuel cell efficiency, it is here proposed to extract the energy electromagnetically from

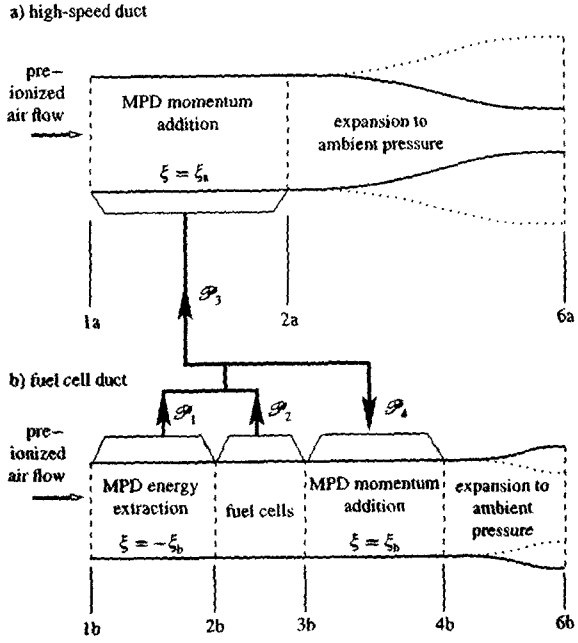

Fig. 1: Schematic of the hypersonic airbreathing Magjet.

the air entering the area where the fuel cells are located, as depicted in Fig. 1. Flow deceleration through electromagnetic energy extraction can result in a much lower temperature increase than would be obtained with standard gasdynamic deceleration.[2-7] Further, it can be achieved in a constant-area duct, hence not requiring significant variations in geometry as the flight Mach number varies. In this way, the air entering the fuel cell stacks can be maintained to a low speed and low temperature, hence minimizing the heat loads.

A foreseen difficulty in decelerating the incoming air is the reduction of the electromagnetic Joule heating, which is expected to significantly affect the performance of the engine and also increase the temperature in the fuel cell compartment. Further, as is shown in Ref. 8, the amount of Joule heating is considerably more difficult to control as the flight Mach number increases to obtain a desired Mach number reduction. Therefore, to minimize as much as possible the impact of Joule heating on the performance of the magjet, the amount of air decelerated electromagnetically is limited to the minimal value needed for the fuel cells to operate. The power extracted from the air as well as the power generated by the fuel cells is then used to accelerate the flow exiting the fuel cell compartment, with a fraction of the power bypassed to the high-speed duct to maximize the engine efficiency.

One objective of this paper is to quantify the optimal amount of power bypassed to the high-speed duct as a function of the Mach number for different values of the mass flow rate ratio between both ducts. A second objective is to assess the impact of Joule heating on the engine performance, which is compared on the basis of the specific impulse to turbojets, ramjets, and scramjets. A third objective is to determine as a function of the flight Mach number the maximal amount of Joule heating in the energy extraction section that would limit the stagnation temperature in the fuel cell compartment to a reasonable level.

The results are obtained through a quasi-one-dimensional model based on the compressible Euler equations including the electromagnetic source terms[9] and neglecting the Hall and ion slip effects. In assessing the performance, it is assumed that the energy conversion efficiency of the fuel cell is of 0.6. While future fuel cells are expected to reach an efficiency approaching 0.7–0.8,[10] it is here preferred to use a value closer to the 0.4–0.5 efficiency exhibited by current fuel cells intended for transportation purposes.[11,12]

Governing Equations

The steady-state quasi-one-dimensional flow equations for a calorically and thermally perfect gas including the electromagnetic source terms can be written as:[8]

$$\frac{\mathrm{d}}{\mathrm{d}x}A\rho q = 0 \tag{1}$$

$$\rho q\frac{\mathrm{d}q}{\mathrm{d}x} + \frac{\mathrm{d}P}{\mathrm{d}x} - \left(\vec{j}\times\vec{B}\right)_x = 0 \tag{2}$$

$$\rho q\frac{\mathrm{d}}{\mathrm{d}x}\left(h+\frac{1}{2}q^2\right) - \frac{\vec{j}\cdot\vec{j}}{\sigma} - q\left(\vec{j}\times\vec{B}\right)_x = 0 \tag{3}$$

where it is assumed that the current density is proportional to the electric field according to Ohm's law without the ion slip and the Hall effects:

$$\vec{E} = \frac{\vec{j}}{\sigma} + \vec{B}\times\vec{v} \tag{4}$$

For simplicity, the electromagnetic Joule heating term $\vec{j}\cdot\vec{j}/\sigma$ and work interaction term $q(\vec{j}\times\vec{B})_x$ shall be referred to in this paper as the "Joule heating" and "work interaction" terms, respectively.

Engine Thrust

High-Speed Duct

In this section, it is desired to determine a general expression for the thrust of the high speed duct for which the flow pressure at the engine exit equals the ambiant pressure. As in Ref. 1 the friction force on the exterior of the engine is neglected, and it is assumed that the pressure is uniform and equal to ambient on the outer surface of the engine. Therefore, the thrust F_a can be written as

$$F_a = \left(\rho_{6a}q_{6a}^2 + P_{6a}\right)A_{6a} - \left(\rho_{1a}q_{1a}^2 + P_{1a}\right)A_{1a} - \left(A_{6a} - A_{1a}\right)P_{1a} \tag{5}$$

Since $P_{6a} = P_{1a}$, the latter becomes:

$$F_a = \left(\rho_{6a}q_{6a}^2\right)A_{6a} - \left(\rho_{1a}q_{1a}^2\right)A_{1a} \tag{6}$$

Each term is now divided by $\dot{m}_a q_{1a}$ to yield:

$$\frac{F_a}{\dot{m}_a q_{1a}} = \frac{q_{6a}}{q_{1a}} - 1 \tag{7}$$

Let's keep the latter on hold for a moment. The difference in total enthalpies between station 1a and 6a can be related to the power input as $H_{6a} - H_{1a} = \mathscr{P}_3/\dot{m}_a$ which, after some algebra, becomes:

$$\frac{2}{(\gamma-1)M_{1a}^2}\left(\frac{T_{6a}}{T_{1a}} - 1\right) + \frac{q_{6a}^2}{q_{1a}^2} - 1 = \frac{2\mathscr{P}_3}{\dot{m}_a q_{1a}^2} \tag{8}$$

But, from Ref. 8, the following relationship exists between the pressure ratio and the temperature ratio:

$$\frac{P_{6a}}{P_{1a}} = \left(\frac{T_{6a}}{T_{1a}}\right)^{\frac{\gamma}{\gamma-1}} [\exp(J_{6a} - J_{1a})]^{\frac{-\gamma}{\gamma-1}} \tag{9}$$

Noting that $P_{6a} = P_{1a}$ and isolating q_{6a}/q_{1a} yields

$$\frac{q_{6a}}{q_{1a}} = \left[\frac{2[1-\exp(J_{6a}-J_{1a})]}{(\gamma-1)M_{1a}^2} + 1 + \frac{2\mathscr{P}_3}{\dot{m}_a q_{1a}^2}\right]^{\frac{1}{2}} \tag{10}$$

which is substituted back into Eq. (7):

$$\frac{F_a}{\dot{m}_a q_{1a}} = \left[\frac{2[1-\exp(J_{6a}-J_{1a})]}{(\gamma-1)M_{1a}^2} + 1 + \frac{2\mathscr{P}_3}{\dot{m}_a q_{1a}^2}\right]^{\frac{1}{2}} - 1 \tag{11}$$

The normalized thrust of the high-speed duct is hence seen to be a function of the specific heat ratio, intake Mach number, normalized power input, and a term related to the amount of Joule heating, $\exp(J_{6a} - J_{1a})$. The latter shall be determined in a following section. But first, let's find the thrust generated by the fuel cell duct.

Fuel Cell Duct

To determine the thrust generated by the fuel cell duct, it is assumed that the flow is isentropic in the fuel cell compartment, between stations 2b and 3b. Further, similarly to the determination of the thrust for the high speed duct, it is assumed that the flow is expanded to ambiant pressure at the duct exit, and that the pressure on the outer surface is equal to the one in the freestream. Then, the thrust can be derived exactly in the same way as in the previous section to yield:

$$\frac{F_b}{\dot{m}_b q_{1b}} = \left[\frac{2[1-\exp(J_{6b}-J_{1b})]}{(\gamma-1)M_{1b}^2} + 1 + \frac{2(\mathscr{P}_4 - \mathscr{P}_1)}{\dot{m}_b q_{1b}^2}\right]^{\frac{1}{2}} - 1 \tag{12}$$

It is emphasized that the latter is derived assuming that the air flows through the fuel cells isentropically without a change in the specific heat ratio or the gas constant. In a practical case, the gas composition as well as the flow stagnation temperature and pressure would certainly vary. Since it is not known at this stage how the latter properties would be altered, it is here chosen to ignore losses originating from that section of the engine.

Combined Thrust

The overall thrust of the magjet corresponds to the sum of the thrust exhibited by both ducts:

$$F = \dot{m}_a q_{1a}\left[\frac{2[1-\exp(J_{6a}-J_{1a})]}{(\gamma-1)M_{1a}^2} + 1 + \frac{2\mathscr{P}_3}{\dot{m}_a q_{1a}^2}\right]^{\frac{1}{2}} + \dot{m}_b q_{1b}\left[\frac{2[1-\exp(J_{6b}-J_{1b})]}{(\gamma-1)M_{1b}^2} + 1 + \frac{2(\mathscr{P}_4 - \mathscr{P}_1)}{\dot{m}_b q_{1b}^2}\right]^{\frac{1}{2}} - \dot{m}_a q_{1a} - \dot{m}_b q_{1b} \tag{13}$$

Noting that the inflow properties are the same for both ducts and that $\mathscr{P}_3 = \Phi(\mathscr{P}_1 + \mathscr{P}_2)$ and that $\mathscr{P}_4 = (1 - \Phi)(\mathscr{P}_1 + \mathscr{P}_2)$, the latter can be rewritten as:

$$\frac{F}{\dot{m}_b q_1} = -1 - \frac{\dot{m}_a}{\dot{m}_b} + \left[\frac{2[1-\exp(J_{6b}-J_{1b})]}{(\gamma-1)M_1^2} + 1 + \frac{2(\mathscr{P}_2(1-\Phi) - \Phi\mathscr{P}_1)}{\dot{m}_b q_1^2}\right]^{\frac{1}{2}} + \frac{\dot{m}_a}{\dot{m}_b}\left[\frac{2[1-\exp(J_{6a}-J_{1a})]}{(\gamma-1)M_1^2} + 1 + \frac{\dot{m}_b}{\dot{m}_a}\frac{2\Phi(\mathscr{P}_1 + \mathscr{P}_2)}{\dot{m}_b q_1^2}\right]^{\frac{1}{2}} \tag{14}$$

At this stage, the terms function of the Joule heating need to be determined as a function of known parameters and flow properties.

Determining $\exp(J_{6a} - J_{1a})$

Since electromagnetic control is only applied between stations a1 and a2 in the high-speed duct, the term $\exp(J_{6a} - J_{1a})$ corresponds to $\exp(J_{2a} - J_{1a})$. From Ref. 8, it is recalled that $\exp(J_{2a} - J_{1a})$ can be expressed as a function of M_{1a} and M_{2a} for a constant-area flow in which ξ is constant:

$$\exp(J_{2a} - J_{1a}) = \left(\frac{b - M_{1a}^2}{b - M_{2a}^2}\right)^{\frac{b-1}{\gamma b}} \left(\frac{M_{1a}}{M_{2a}}\right)^{\frac{2}{\gamma b}} \tag{15}$$

where b is a function of the specific heat ratio and ξ:

$$b \equiv \frac{(\gamma+1)(\xi+1) - 2\gamma\xi}{\gamma\xi(\gamma-1)} \tag{16}$$

To determine $\exp(J_{2a} - J_{1a})$ in Eq. (15), M_{2a} needs to be determined. This can be accomplished by noting that the total enthalpy change from station 1a to station 2a corresponds to the ratio between the power input and the mass flow rate:

$$\dot{m}_a H_{2a} = \dot{m}_a H_{1a} + \mathscr{P}_3 \tag{17}$$

or, expanding the total enthalpy as $C_P T + q^2/2$ and dividing both sides by $\dot{m}_a C_P T_{1a}$:

$$\frac{T_{2a}}{T_{1a}}\left(1 + \frac{\gamma-1}{2}M_{2a}^2\right) = 1 + \frac{\gamma-1}{2}M_{1a}^2 + \frac{\mathscr{P}_3}{C_P T_{1a}\dot{m}_a} \tag{18}$$

where the temperature ratio can be expressed as a function of M_{2a}, M_{1a}, ξ, and γ for a constant area flow in which the ratio between the Joule heating and the work interaction term is constant:[8]

$$\frac{T_{2a}}{T_{1a}} = \left(\frac{b-M_{1a}^2}{b-M_{2a}^2}\right)^{\frac{2(b-1)}{b(\gamma+1)}} \left(\frac{M_{1a}}{M_{2a}}\right)^{\frac{(\gamma-1)2b+4}{b(\gamma+1)}} \tag{19}$$

Substituting the latter in the former, and noting that $\mathscr{P}_3 = \Phi(\mathscr{P}_1 + \mathscr{P}_2)$, and that both ducts share the same inflow properties, the following is obtained:

$$\left(\frac{b-M_{1a}^2}{b-M_{2a}^2}\right)^{\frac{2(b-1)}{b(\gamma+1)}} \left(\frac{M_{1a}}{M_{2a}}\right)^{\frac{(\gamma-1)2b+4}{b(\gamma+1)}} \left(1+\frac{\gamma-1}{2}M_{2a}^2\right) = 1+\frac{\gamma-1}{2}M_{1a}^2\left(1+\frac{\dot{m}_b}{\dot{m}_a}\frac{2\Phi(\mathscr{P}_1+\mathscr{P}_2)}{\dot{m}_b q_{1b}^2}\right) \tag{20}$$

which yields M_{2a} knowing the inflow Mach number, specific heat ratio, ξ, and the normalized power generation terms. The Mach number at station 2a can then be substituted in Eq. (15) to obtain $\exp(J_{6a} - J_{1a})$.

Determining $\exp(J_{6b} - J_{1b})$

The term related to the amount of Joule heating in the fuel cell duct corresponds to the product of the Joule heating-related terms between stations 1b-2b and stations 3b-4b:

$$\exp(J_{6b} - J_{1b}) = \exp(J_{2b} - J_{1b})\exp(J_{4b} - J_{3b}) \tag{21}$$

where both terms on the RHS are taken from Ref. 8:

$$\exp(J_{2b} - J_{1b}) = \left(\frac{b-M_{1b}^2}{b-M_{2b}^2}\right)^{\frac{b-1}{\gamma b}} \left(\frac{M_{1b}}{M_{2b}}\right)^{\frac{2}{\gamma b}} \tag{22}$$

$$\exp(J_{4b} - J_{3b}) = \left(\frac{b-M_{3b}^2}{b-M_{4b}^2}\right)^{\frac{b-1}{\gamma b}} \left(\frac{M_{3b}}{M_{4b}}\right)^{\frac{2}{\gamma b}} \tag{23}$$

in which M_{2b} is here a user-specified constant. It is recalled that the flow properties remain constant in the fuel cell compartment, so that $M_{3b} = M_{2b}$. The value of M_{4b} can be found as a function of M_{3b} and b similarly as M_{2a} was obtained in Eq. (20):

$$\left(\frac{b-M_{3b}^2}{b-M_{4b}^2}\right)^{\frac{2(b-1)}{b(\gamma+1)}} \left(\frac{M_{3b}}{M_{4b}}\right)^{\frac{(\gamma-1)2b+4}{b(\gamma+1)}} \left(1+\frac{\gamma-1}{2}M_{4b}^2\right) = 1+\frac{\gamma-1}{2}M_{3b}^2\left(1+\frac{M_{1b}^2 T_{1b}}{M_{3b}^2 T_{3b}}\frac{2(1-\Phi)(\mathscr{P}_1+\mathscr{P}_2)}{\dot{m}_b q_{1b}^2}\right) \tag{24}$$

where $\mathscr{P}_4 = (1-\Phi)(\mathscr{P}_1 + \mathscr{P}_2)$. For a constant area flow between station 1b and 3b, T_{1b}/T_{3b} can be expressed as:[8]

$$\frac{T_{1b}}{T_{3b}} = \frac{T_{1b}}{T_{2b}} = \left(\frac{M_{2b}}{M_{1b}}\right)^{\frac{2(\gamma-1)}{\gamma+1}} [\exp(J_{2b} - J_{1b})]^{\frac{-2\gamma}{\gamma+1}} \tag{25}$$

Eq. (24) hence yields M_{4b} knowing the Mach number in the fuel cell section, the specific heat ratio, ξ, and the normalized power generation terms. The Mach number at station 4b can then be substituted in Eq. (23) to obtain $\exp(J_{4b} - J_{3b})$. Then, the terms $\exp(J_{4b} - J_{3b})$ and $\exp(J_{2b} - J_{1b})$ can be substituted in Eq. (21) to obtain $\exp(J_{6b} - J_{1b})$. However, in order to close the equations, the normalized power generation terms $\mathscr{P}_1/\dot{m}_b q_{1b}^2$ and $\mathscr{P}_2/\dot{m}_b q_{1b}^2$ must be determined.

Determining the Normalized Power Generation Terms

The power extracted in the energy extraction section can be obtained from Eq. (20), isolating the normalized power extracted $\mathscr{P}_1$:

$$\frac{\mathscr{P}_1}{\dot{m}_b q_{1b}^2} = \frac{1}{2} - \frac{1}{(\gamma-1)M_{1b}^2}\left[-1+\left(\frac{b-M_{1b}^2}{b-M_{2b}^2}\right)^{\frac{2(b-1)}{b(\gamma+1)}} \left(\frac{M_{1b}}{M_{2b}}\right)^{\frac{(\gamma-1)2b+4}{b(\gamma+1)}} \left(1+\frac{\gamma-1}{2}M_{2b}^2\right)\right] \tag{26}$$

with all the terms on the RHS being user-specified. To determine $\mathscr{P}_2$, it is assumed that the entire amount of oxygen flowing in the fuel cell duct is used by the fuel cells to generate electricity. The power generated by the fuel cells would hence correspond to the product of the fuel cell efficiency η_{fc} by the fuel specific energy e_f and by the mass flow rate of the fuel:

$$\mathscr{P}_2 = \dot{m}_{fuel}\eta_{fc}e_f \tag{27}$$

Noting that $\dot{m}_{fuel} = \dot{m}_b\phi_s$, the latter can be rewritten to:

$$\frac{\mathscr{P}_2}{\dot{m}_b q_{1b}^2} = \frac{1}{M_{1b}^2}\frac{\phi_s\eta_{fc}e_f}{a_{1b}^2} \tag{28}$$

where ϕ_s is the stoichiometric mass fraction between the fuel and the air. Since hydrogen is the chosen fuel, ϕ_s and e_f are hereafter set to 0.03 and 142 MJ/kg,[13] respectively.

Maximum Allowable Amount of Joule Heating in the Energy Extraction Section

In this section, it is desired to find the value of ξ_b that would result in a fixed maximal stagnation temperature in the fuel cell compartment. From Ref. 8, the temperature ratio can be written as a function of the Mach number between stations 1b and 2b:

$$\frac{T_{2b}}{T_{1b}} = \left(\frac{b-M_{1b}^2}{b-M_{2b}^2}\right)^{\frac{2(b-1)}{b(\gamma+1)}} \left(\frac{M_{1b}}{M_{2b}}\right)^{\frac{(\gamma-1)2b+4}{b(\gamma+1)}} \tag{29}$$

Noting that the ratio between the stagnation and static temperature at station 2b corresponds to:

$$\frac{T_{2b}^\circ}{T_{2b}} = 1+\frac{\gamma-1}{2}M_{2b}^2 \tag{30}$$

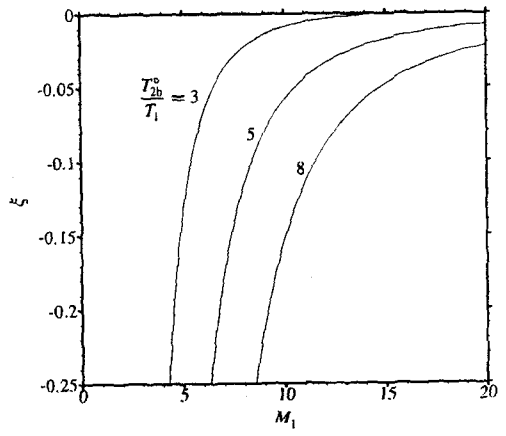

Fig. 2: Value of $\xi = -\xi_b$ in the energy extraction section to obtain a desired ratio between the stagnation temperature at the fuel cell entrance and the incoming air temperature, as specified in Eq. (31); γ and M_{2b} are set to 1.4 and 1.0 respectively.

from which T_{2b} is isolated and substituted in the former equation to yield:

$$\frac{T_{2b}^{\circ}}{T_1} = \left(1 + \frac{\gamma - 1}{2} M_{2b}^2\right)\left(\frac{b - M_1^2}{b - M_{2b}^2}\right)^{\frac{2(b-1)}{b(\gamma+1)}}\left(\frac{M_1}{M_{2b}}\right)^{\frac{(\gamma-1)2b+4}{b(\gamma+1)}} \tag{31}$$

From the latter, b can be determined for a known M_{2b}, intake Mach number, and ratio between the stagnation temperature in the fuel cell compartment and the freestream temperature. From b, ξ can be obtained from Eq. (16). In this paper, the Mach number in the fuel cell compartment is fixed to 1.0, which corresponds to the choking point for MPD energy extraction in a constant-area duct.[8]

The value of ξ in the energy extraction device is plotted in Fig. 2 as a function of the Mach number and the ratio between the stagnation temperature at the entrance of the fuel cell compartment and the incoming air temperature. Since energy extraction is only performed when the incoming Mach number is higher than 1.0, ξ is set to $-\xi_b$ in the energy extraction section when $M_1 > 1.0$ and to zero otherwise. As Fig. 2 shows, a relatively high magnitude of ξ_b in the range 0.10–0.25 is restrictive on the maximum flight Mach number attainable. Indeed, the maximal flight Mach number can not exceed 6–8 for a fuel cell compartment entrance stagnation temperature 5 times the flow incoming temperature. Meanwhile, upon reducing ξ_b to 0.01, it is possible to attain a flight Mach number in excess of 15.

For the remainder of this paper, ξ_b is typically set to 0.25 although lower values shall also be investigated. While it might be technically difficult to lower the Joule heating down to ten percent or even one percent of the work interaction, this is here seen to be a necessary constraint to maintain the stagnation temperature to a reasonable level in the fuel cell compartment at a high hypersonic Mach number.

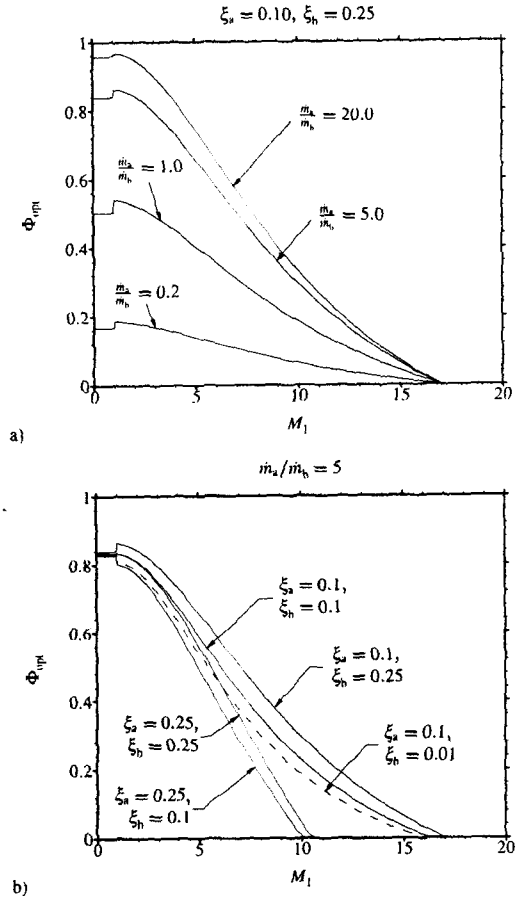

Fig. 3: Optimal power bypass ratio Φ_{opt} as a function of the Mach number, with $M_{2b} = 1.0$, $\gamma = 1.4$, and $\phi_s \eta_{fc} e_f / a_1^2 = 26.06$, which is found assuming that the fuel is hydrogen, the inflow temperature is set to 245 K, and the fuel cell efficiency is set to 0.6.

Optimal Value of the Power Bypass Ratio

The ratio of the power bypassed to the high-speed duct, Φ, is determined such that the thrust is maximized keeping constant the user-specified parameters such as the intake Mach number, ξ, the fuel cell efficiency, etc. The optimal value for Φ is hence determined iteratively by finding the maximal thrust in the range $0 < \Phi < 1$ yielding the optimal power bypass ratio, with the latter being a function of:

$$\Phi_{opt} = f_1\left(\gamma, \frac{\phi_s \eta_{fc} e_f}{a_1^2}, M_{2b}, M_1, \xi_a, \xi_b, \frac{\dot{m}_b}{\dot{m}_a}\right) \tag{32}$$

where ξ_a is the ratio between the electromagnetic Joule and work interaction terms in the high-speed duct, while ξ is set to $-\xi_b$ and ξ_b before and after the fuel cell compartment, respectively.

In Fig. 3, it can be seen that an increase in the flight Mach number induces a considerable Φ_{opt} reduction,

especially when the mass flow rate ratio is high. This is to be expected, as the thrust is sensitive to the mass flow rate for a small intake Mach number.[1] For this reason, a high mass flow rate ratio induces a significant fraction of the power bypassed to the high-speed duct. On the other hand, as the flight Mach number increases, it becomes more efficient for the power to be added to the slow speed flow exiting the fuel cell compartment, due to the thrust becoming progressively more sensitive to the flow speed rather than the mass flow rate.[1]

Keeping the mass flow rate ratio constant to 5, Fig. 3b shows the impact of ξ_a and ξ_b on the optimal power bypass ratio. For a given value of ξ_b, it is apparent that an increase in the value of ξ_a translates into a decrease of the optimal fraction of the power delivered to the high-speed duct. This trend can be explained as follows: as ξ_a increases, a larger fraction of the power input to the high-speed duct gets converted into heat rather than work; since the heat addition process is not performed at a pressure significantly higher than ambient, it does not result into thrust; therefore, Φ_{opt} decreases such that less power is allocated to the relatively less performant high-speed duct. As expected, the opposite trend is observed when ξ_a is kept constant and ξ_b is increased. It can hence be observed that a Joule heating increase in either duct translates into less power transferred to that part of the engine.

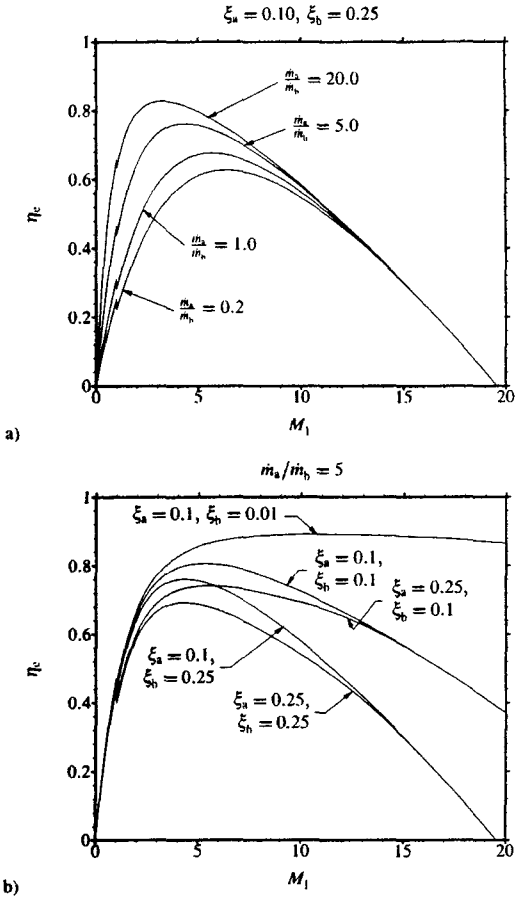

Fig. 4: Engine efficiency as a function of the Mach number according to Eq. (34), with $M_{2b} = 1.0$, $\gamma = 1.4$, and $\phi_s \eta_{fc} e_f / a_1^2 = 26.06$, which is determined assuming that the fuel is hydrogen, the inflow temperature corresponds to 245 K, and the fuel cell efficiency is set to 0.6.

Engine Efficiency

The engine efficiency is here defined as in Ref. 1, that is, as the ratio between the thrust of the engine multiplied by the flight speed and the power generated by the fuel cells:

$$\eta_e \equiv \frac{F q_1}{\mathscr{P}_2} \tag{33}$$

Substituting Eq. (14) in the latter, the engine efficiency takes on the form:

$$\begin{aligned}\eta_e = \frac{\dot{m}_b q_1^2}{\mathscr{P}_2}\Bigg[&\frac{2[1-\exp(J_{6b}-J_{1b})]}{(\gamma-1)M_1^2}+1 \\ &+\frac{2(\mathscr{P}_2(1-\Phi)-\Phi\mathscr{P}_1)}{\dot{m}_b q_1^2}\Bigg]^{\frac{1}{2}}-1 \\ &+\frac{\dot{m}_a}{\dot{m}_b}\Bigg[\frac{2[1-\exp(J_{6a}-J_{1a})]}{(\gamma-1)M_1^2}+1 \\ &+\frac{\dot{m}_b}{\dot{m}_a}\frac{2\Phi(\mathscr{P}_1+\mathscr{P}_2)}{\dot{m}_b q_1^2}\Bigg]^{\frac{1}{2}}-\frac{\dot{m}_a}{\dot{m}_b}\end{aligned} \tag{34}$$

which is a function of the following variables:

$$\eta_e = f_2\left(\gamma, \frac{\phi_s \eta_{fc} e_f}{a_1^2}, M_{2b}, M_1, \xi_a, \xi_b, \frac{\dot{m}_b}{\dot{m}_a}\right) \tag{35}$$

The engine efficiency can be seen not to be a function directly of the power bypass ratio but rather of $\phi_s \eta_{fc} e_f / a_1^2$. This is due to Φ being set at all times to its optimal value which depends on some of the parameters that the engine efficiency depends on but is also a function of $\phi_s \eta_{fc} e_f / a_1^2$.

In Fig. 4a, the efficiency is plotted for values of ξ_a and ξ_b set to 0.10 and 0.25 respectively, while the mass flow rate ratio between the fuel cell duct and the high speed duct is varied from 0.2 to 20. The mass flow rate ratio is seen to have a decreasing impact on the engine efficiency as the flight Mach number increases, due to the power bypassed to the high-speed duct being very small at high Mach number. However, at a lower flight Mach number where Φ is high, a high mass flow rate ratio is seen to result in a two- to three-fold increase in the engine efficiency.

Keeping the mass flow rate ratio constant to 5, Fig. 4b shows the impact of ξ_a and ξ_b on the efficiency. As the flight Mach number is increased, the efficiency is observed to be progressively more sensitive to ξ_b rather than ξ_a. This is postulated to be due to a combination of three phenomena: (i) as outlined previously, most of the power generated at a high flight Mach number

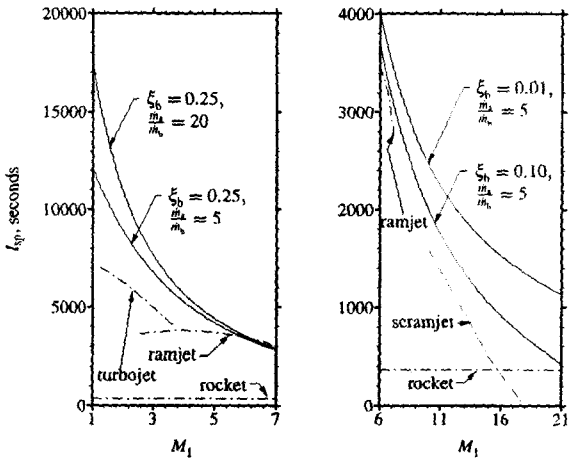

Fig. 5: Specific impulse versus the flight Mach number according to Eq. (37); ξ_a is set to 0.1, the fuel cell efficiency to 0.6, and T_1 to 245 K; except for the H_2-O_2 rocket, all engines are airbreathing and use H_2 as fuel.

is not bypassed to the high-speed duct, but is rather added to the low-speed flow downstream of the fuel cells, (ii) the amount of energy extracted from the flow increases along with the flight Mach number, and (iii) the amount of Joule heating in the fuel cell duct increases proportionally to the product between ξ_b and the sum of the energy extracted and added as work before and after the fuel cell compartment. Therefore, as the Mach number increases, the efficiency becomes mostly a function of the amount of Joule heating present in the fuel cell duct. On the other hand, when the flight Mach number is low, the amount of Joule heating in the high-speed duct plays a more predominant role due to the high power bypass ratio and the small amount of energy extracted.

Specific Impulse

By definition, the specific impulse corresponds to the ratio between the engine thrust and the fuel mass flow rate times the gravitational acceleration:

$$I_{sp} \equiv \frac{F}{\dot{m}_{fuel} g} \tag{36}$$

Noting that $\dot{m}_{fuel} = \dot{m}_b \phi_s$, the latter can be rewritten to:

$$I_{sp} \equiv \frac{F}{\dot{m}_b \phi_s g} = \frac{F q_1 \mathscr{P}_2}{q_1 \mathscr{P}_2 \dot{m}_b \phi_s g} = \frac{\mathscr{P}_2}{\dot{m}_b q_1^2} \frac{\eta_c q_1}{\phi_s g} = \frac{\eta_{fc} e_f}{a_1 g} \frac{\eta_c}{M_1} \tag{37}$$

where $\mathscr{P}_2$ is taken from Eq. (28). The specific impulse is hence a function of the following variables:

$$I_{sp} = f_3\left(\gamma, \frac{\phi_s \eta_{fc} e_f}{a_1^2}, \frac{\eta_{fc} e_f}{a_1 g}, M_{2b}, M_1, \xi_a, \xi_b, \frac{\dot{m}_b}{\dot{m}_a}\right) \tag{38}$$

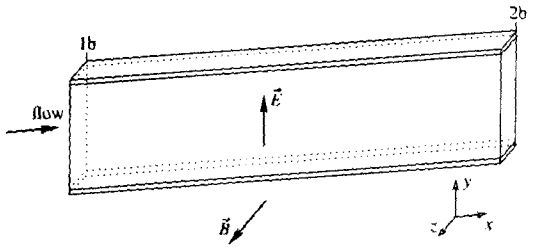

Fig. 6: Schematic of the energy extraction section part of the fuel cell duct. The magnetic and electric field vectors are perpendicular to the velocity vector and to one another to minimize the Joule heating.

The latter is shown in Fig. 5 and compared to the one of a turbojet, ramjet, scramjet, and rocket over their respective range of operation. Throughout the Mach number range 1–15, the specific impulse of the magjet is typically 1.5–3 times the one of airbreathing chemical engines.

As was shown in a previous section, in order to limit the stagnation temperature in the fuel cell compartment to five times the freestream temperature, it is necessary to fix ξ_b to at the most 0.10–0.25 when the inflow Mach number is less than 6–8, and to as low as 0.01 when the inflow Mach number increases to 20. As can be seen from Fig. 5, decreasing ξ_b also has the advantage of increasing significantly the specific impulse at higher speeds, with a magjet specific impulse being 5 times the one of the scramjet or the rocket at Mach 15.

Although not shown in Fig. 5, it is noted that a change in the mass flow ratio does not affect significantly the specific impulse for a flight Mach number in excess of 6 due to very little power being bypassed to the high speed duct. However, at a lower Mach number, a higher mass flow ratio is beneficial in increasing the specific impulse, with the maximal observed increase being of about 45% at Mach 1 for a fourfold increase in the mass flow ratio.

Electromagnetic Properties in the Energy Extraction Section

In this section, the electromagnetic properties are evaluated in the energy extraction section part of the fuel cell compartment. In order to minimize the Joule heating, the electric and magnetic fields are positioned perpendicular to one another and to the velocity vector, as depicted in Fig. 6. In Ref. 8, an expression for $\sigma B_z^2 (x_{2b} - x_{1b})/\rho_1 q_1$ as a function of γ, ξ and the Mach numbers at stations 1b and 2b is outlined, for the special case of a constant ξ, magnetic field, and electrical conductivity. Noting that the dynamic pressure corresponds to $\rho_1 q_1^2/2$, the normalized magnetic field term can be rewritten to:

$$\frac{\sigma B_z^2 (x_{2b} - x_{1b})}{\rho_1 q_1} = \frac{\sigma B_z^2 (x_{2b} - x_{1b}) M_1 a_1}{2 P_{dyn}} \tag{39}$$

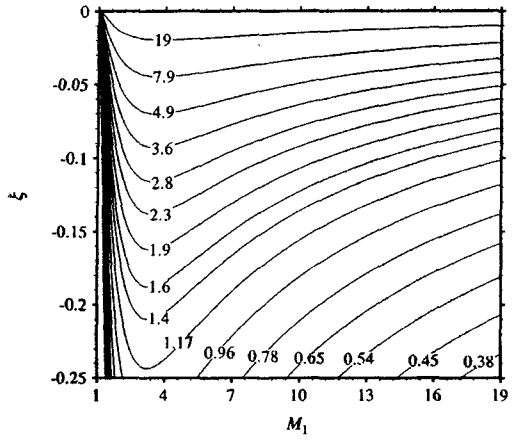

Fig. 7: Contour levels of $\sigma B_z^2(x_{2b}-x_{1b})a_1/P_{dyn}$ in the energy extraction section, as outlined in Eq. (40), with the specific heat ratio fixed to 1.4; appropriate units for σ, B_z, x, P_{dyn}, and a_1 are mho/meter, Tesla, meter, Pascal, and meter/second respectively.

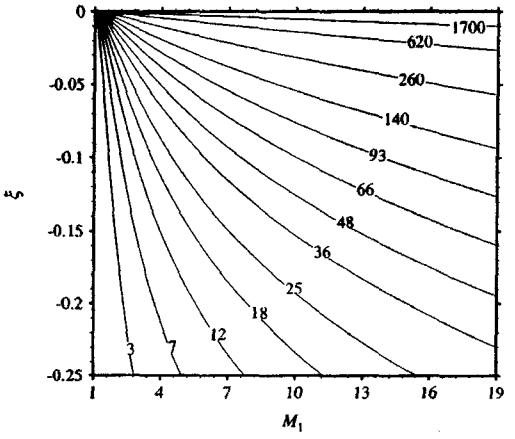

Fig. 8: Contour levels of $\sigma E_y^2(x_{2b}-x_{1b})/P_{dyn}a_1$ in the energy extraction section according to Eq. (42), with the specific heat ratio fixed to 1.4; appropriate units for σ, E_y, x, P_{dyn}, and a_1 are mho/meter, Volt/meter, meter, Pascals, and meter/second respectively.

Substituting the latter in the expression for $\sigma B_z^2(x_{2b}-x_{1b})/\rho_1 q_1$ in Ref. 8, the following can be obtained:

$$\frac{\sigma B_z^2(x_{2b}-x_{1b})}{P_{dyn}/a_1} = \frac{2b\gamma+2}{b(\gamma+1)\xi\gamma M_1} \times \ln\left[\left(\frac{M_{2b}^2(b-M_1^2)}{M_1^2(b-M_{2b}^2)}\right)^{\frac{b-1}{b}} \frac{\exp(M_{2b}^{-2})}{\exp(M_1^{-2})}\right] \quad (40)$$

which yields the normalized magnetic field term given ξ, γ, M_1 and M_{2b}. On the other hand, should the electric field be constant throughout the energy extraction section with the magnetic field varied, an expression for $\sigma E_y^2(x_{2b}-x_{1b})/P_1 q_1$ can be found in Ref. 8 as a function of M_1, M_{2b}, γ, and ξ. Rewriting this term as a function of the dynamic pressure yields

$$\frac{\sigma E_y^2(x_{2b}-x_{1b})}{P_1 q_1} = \frac{\sigma E_y^2(x_{2b}-x_{1b})\gamma M_1}{2a_1 P_{dyn}} \quad (41)$$

Upon substituting the latter into the expression for the normalized electric field,[8] it can be stated that:

$$\frac{\sigma E_y^2(x_{2b}-x_{1b})}{P_{dyn}a_1} = \frac{2(\xi+1)}{\xi(\gamma-1)M_1}\left[-1-\frac{\gamma-1}{2}M_1^2 + \left(1+\frac{\gamma-1}{2}M_2^2\right)\left(\frac{b-M_1^2}{b-M_2^2}\right)^{\frac{2(b-1)}{b(\gamma+1)}}\left(\frac{M_1}{M_2}\right)^{\frac{(\gamma-1)2b+4}{b(\gamma+1)}}\right] \quad (42)$$

The normalized magnetic and electric field terms are plotted in Figs. 7 and 8 for an inflow Mach number varying from 1.0 to 19 and a magnitude of ξ not exceeding 0.25. In the analysis that follows, it is assumed that the dynamic pressure and the entrance sound speed are not a strong function of the inflow Mach number. The assumption of a constant sound speed is excellent as the air temperature does not vary much throughout the atmosphere.[14] Further, maintaining a constant dynamic pressure flight path is desirable for high-speed flight vehicles in order to keep the heat loads and fluid forces on the vehicle within a reasonable range. It can be seen that for a constant incoming sound speed and dynamic pressure, the normalized magnetic field term generally decreases as the incoming flow Mach number increases for a given ξ. This is postulated to be due primarily to the decrease in flow density for an increase in flight Mach number at constant dynamic pressure. However, the opposite trend is observed for the electric field, which is seen to increase along with the flight Mach number. This is attributed to the electric field scaling in magnitude approximately in proportion to the product between the magnetic field and the flow speed,[8] with the latter increasing at a faster rate than the magnetic field decreases.

A striking aspect of the normalized magnetic and electric field terms is their very high dependence on ξ, especially at a high Mach number. More precisely, both the normalized magnetic and electric field terms increase approximately fifty-fold for ξ varied from -0.25 to -0.01 when the flow Mach number is greater than 10. This is particularly troublesome as a low magnitude of ξ is necessary at high Mach number to limit the flow stagnation temperature in the fuel cell compartment. It can hence be seen that a combination of a very high magnetic field, electric field, electrical conductivity, and length of the energy extraction section would be required to limit the stagnation temperature in the fuel cell compartment to a reasonable value when the incoming Mach number is high. While there is hope that advances in superconductors can yield magnets generating a high magnetic field strength, the latter would necessarily induce a high electric field when the amount of Joule heating is small. Indeed, the electric field vector must approach the vector $\vec{B}\times\vec{v}$ both in

terms of magnitude and orientation in order to minimize ξ.[8] However, the electric field cannot be too high as sparks would form, and the length of the energy extraction section cannot be too high as this would increase the boundary layer height hence increasing the possibility of flow reversal. For the latter two reasons, it can be deduced that a very high electrical conductivity is necessary in the energy extraction section for airbreathing flight in the high hypersonic range.

Conclusions

To limit the stagnation temperature of the air flowing through the fuel cells, it is seen to be crucial to lower the magnitude of the ratio between the Joule heating and work interaction terms in the energy extraction section prior to the fuel cell compartment. Beyond a flight Mach number of 15, the ratio must be decreased below 0.01 to limit the air stagnation temperature in the fuel cells to 5 times the freestream temperature. Additionally to being crucial in limiting the air stagnation temperature in the fuel cell compartment, the amount of Joule heating affects the engine efficiency considerably at high Mach number, while exhibiting a much reduced impact at lower speed. For instance, a decrease in the Joule heating / work ratio from 0.25 to 0.01 induces a rise in the engine efficiency from 0 to 0.86 at Mach 20, but of only 10% at Mach 3.

While it is seen to be possible to obtain a high engine efficiency and a low air stagnation temperature in the fuel cell compartment up to a flight Mach number of 15 by limiting the Joule heating to 1% of the work interaction, it is cautioned that this might be very difficult to achieve in practice as a small value of the Joule heating necessarily increases the required magnetic and electric field strength, as well as the flow conductivity. But more importantly, such a small amount of Joule heating requires the magnitude of the product between the speed and the magnetic field to be within 1% of the magnitude of the electric field.[8] In an actual engine, the speed disturbances in the flow due to the boundary layer or atmospheric non-uniformities are expected to make it difficult to decrease the Joule heating to that level. *Should it not be possible to decrease the Joule heating / work ratio below 0.25, an airbreathing magjet engine would not be able to operate beyond Mach 6.5 without raising the air stagnation temperature in the fuel cell compartment to more than 5 times the incoming temperature.*

Along a constant-dynamic-pressure flight path, the product of the square of the electric field and the electrical conductivity is seen to increase considerably in the energy extraction section of the fuel cell duct when (i) the flight Mach number increases, and (ii) when the magnitude of the ratio between the Joule heating and work interaction term decreases. This is particularly problematic since it is necessary to minimize the Joule heating as the Mach number increases in order to maintain the stagnation temperature of the air in the fuel cell compartment to a reasonable level. Since the electric field cannot be too high as sparks would form, *an elevated level of electrical conductivity is expected for flight in the high hypersonic regime.*

For a flight Mach number lower than 8, the mass flow rate ratio between the high-speed and fuel cell ducts is seen to affect considerably the engine efficiency, with the latter increasing by as much as 3 times for a mass flow rate ratio increased from 0.2 to 20. At higher flight Mach number, varying the mass flow rate ratio between the same bounds affects the engine efficiency by less than 10%. The optimal power bypass ratio is also observed to be significantly less sensitive to a change in the mass flow rate ratio in the hypersonic range. Based on these observations, it can be concluded that *a high mass flow rate in the high-speed duct is important to the performance of the magjet at lower Mach number but not necessary when the latter exceeds 8–10.*

Acknowledgements

This work has been supported by the BK21 program and by the Natural Sciences and Engineering Research Council of Canada.

References

1) Parent, B. and Jeung, I. S., "Quasi One-Dimensional Performance Analysis of a Magnetoplasma Jet Engine," *Journal of Propulsion and Power*, submitted in Oct. 2003, can be downloaded online at `ftp://147.46.241.213/magjet.pdf`.

2) Gurijanov, E. P. and Harsha, P. T., "AJAX: New Directions in Hypersonic Technology," 1996, AIAA Paper 96-4609.

3) Kopchenov, V., Vatazhin, A., and Gouskov, O., "Estimation of Possibility of Use of MHD Control in Scramjet," 1999, AIAA Paper 99-4971.

4) Lee, Y.-M., Czysz, P. A., and Petley, D., "Magnetohydrodynamic Energy Bypass Applications for Single Stage-to-Orbit Vehicles," 2001, AIAA Paper 2001-1901.

5) Brichkin, D. I., Kuranov, A. L., and Sheikin, E. G., "Scramjet with MHD Control Under "AJAX" Concept. Physical Limitations." 2001, AIAA Paper 2001-0381.

6) Litchford, R. J., Cole, J. W., Bityurin, V. A., and Lineberry, J. T., "Thermodynamic Cycle Analysis of Magnetohydrodynamic-Bypass Hypersonic Airbreathing Engines," *Journal of Propulsion and Power*, Vol. 17, No. 2, 2001, Technical Notes.

7) Poggie, J., "Numerical Simulation of Electromagnetic Flow Control for Hypersonic Systems," Sept. 2002, AIAA Paper 2002-5182, presented at the 11th International Space Planes and Hypersonic Technologies conference, Orléans, France.

8) Parent, B. and Jeung, I. S., "Effect of Joule Heating on the Performance of Magnetoplasmadynamic Energy Extraction Systems," *Journal of Propulsion and Power*, submitted in Oct. 2003, can be downloaded online at `ftp://147.46.241.213/jouleheating.pdf`.

9) Sutton, G. W. and Sherman, A., *Engineering Magnetohydrodynamics*, McGraw-Hill, New-York, NY, 1965.

10) Song, C., "Fuel Processing for Low-Temperature and High-Temperature Fuel Cells. Challenges, and Opportunities for Sustainable Development in the 21st Century," *Catalysis Today*, Vol. 77, 2002, pp. 17–49.

11) Folkesson, A., Andersson, C., Alvfors, P., Alakula. M., and Overgaard, L., "Real Life Testing of a Hybrid PEM Fuel Cell Bus," *Journal of Power Sources*, Vol. 118, 2003, pp. 349–357.

12) Godat, J. and Marechal, F., "Optimization of a Fuel Cell System Using Process Integration Techniques," *Journal of Power Sources*, Vol. 118, 2003, pp. 411–423.

13) Aubrecht, G., *Energy*, Prentice Hall, 2nd ed., 1995.

14) U.S. Government Printing Office, Washington, D.C., *The U.S. Standard Atmosphere (1962)*, 1962.